Lysophospholipases cooperate to mediate lipid homeostasis and lysophospholipid signaling[S]

James A. Wepy,* James J. Galligan,† Philip J. Kingsley,† Shu Xu,† Michael C. Goodman,* Keri A. Tallman,*,§ Carol A. Rouzer,,†† and Lawrence J. Marnett[1,*,†,§,**,††]**

A. B. Hancock Jr. Memorial Laboratory for Cancer Research, Departments of Chemistry,* Biochemistry,† and Pharmacology,§ Vanderbilt Institute of Chemical Biology,** and Vanderbilt-Ingram Cancer Center,†† Vanderbilt University School of Medicine, Nashville, TN 37232-0146

ORCID IDs: 0000-0002-9124-6078 (J.A.W.); 0000-0002-5612-0680 (J.J.G.)

Abstract Lysophospholipids (LysoPLs) are bioactive lipid species involved in cellular signaling processes and the regulation of cell membrane structure. LysoPLs are metabolized through the action of lysophospholipases, including lysophospholipase A1 (LYPLA1) and lysophospholipase A2 (LYPLA2). A new X-ray crystal structure of LYPLA2 compared with a previously published structure of LYPLA1 demonstrated near-identical folding of the two enzymes; however, LYPLA1 and LYPLA2 have displayed distinct substrate specificities in recombinant enzyme assays. To determine how these in vitro substrate preferences translate into a relevant cellular setting and better understand the enzymes' role in LysoPL metabolism, CRISPR-Cas9 technology was utilized to generate stable KOs of *Lypla1* and/or *Lypla2* in Neuro2a cells. Using these cellular models in combination with a targeted lipidomics approach, LysoPL levels were quantified and compared between cell lines to determine the effect of losing lysophospholipase activity on lipid metabolism.[JLR] This work suggests that LYPLA1 and LYPLA2 are each able to account for the loss of the other to maintain lipid homeostasis in cells; however, when both are deleted, LysoPL levels are dramatically increased, causing phenotypic and morphological changes to the cells.—Wepy, J. A., James J. Galligan, P. J. Kingsley, S. Xu, M. C. Goodman, K. A. Tallman, C. A. Rouzer, and L. J. Marnett. **Lysophospholipases cooperate to mediate lipid homeostasis and lysophospholipid signaling. *J. Lipid Res.* 2019.** 60: **360–374.**

Supplementary key words brain lipids • eicosanoids • prostaglandins • fatty acid • protein kinases/MAP kinase • lipidomics • mass spectrometry • fluorescence microscopy • neurons • X-ray crystallography

Lysophospholipids (LysoPLs) are detergent-like lipid species that play a critical role in a wide variety of cellular signaling mechanisms in addition to maintaining the structure, shape, and fluidity of cell membranes (1–3). Each LysoPL comprises one nonpolar acyl chain, varying in length and degree of unsaturation, and a polar glycerophosphate headgroup. Based on the structure of the headgroup, LysoPLs belong primarily to one of six classes, including lysophosphatidic acids (LPAs), lysophosphatidylcholines (LPCs), lysophosphatidylethanolamines (LPEs), lysophosphatidylglycerols (LPGs), lysophosphatidylinositols (LPIs), and lysophosphatidylserines (LPSs), each with distinct biological functions dependent on physiological location and availability of their respective cellular receptors.

LysoPLs have been shown to elicit a wide range of biological effects, including cell proliferation, intracellular calcium mobilization, metabolic activity, inflammatory and antiinflammatory processes, and neuritogenesis (4–20). These effects are generally evoked through ligand-receptor interactions, but this is not always the case. For example, high physiological concentrations of LPCs (~200 μM in human plasma) call into question a receptor agonist role in some circumstances, and accruing evidence supports the hypothesis that they can elicit effects by altering membrane properties or interacting directly with proteins in ways other than saturable binding to a specific site (21–24). For example, LPCs have been shown to directly promote Ras-mediated activation of the MAPK signaling pathway by a mechanism that does not involve characterized LysoPL receptors (17). In contrast, LPEs, LPGs, and LPIs have also been shown to activate this signaling pathway, but they

This work was supported by National Institutes of Health Grants CA089450 and T32-ES007028; the Hancock Jr. Memorial Cancer Center Fund; and National Institute of General Medical Sciences Fellowship Ruth L. Kirschstein National Research Service Award 5F31GM120879-02. Its contents are solely the responsibility of the authors and do not necessarily represent the official views of the National Institutes of Health.

Manuscript received 19 June 2018 and in revised form 5 November 2018.

Published, JLR Papers in Press, November 27, 2018
DOI https://doi.org/10.1194/jlr.M087890

Abbreviations: CST, Cell Signaling Technologies; DKO, double KO; LPA, lysophosphatidic acid; LPC, lysophosphatidylcholine; LPE, lysophosphatidylethanolamine; LPG, lysophosphatidylglycerol; LPI, lysophosphatidylinositol; LPS, lysophosphatidylserine; LYPLA1, lysophospholipase A1; LYPLA2, lysophospholipase A2; LysoPL, lysophospholipid; MEK, MAPK/ERK kinase; PDB, Protein Data Bank; PFB, pentafluorobenzyl; PG, prostaglandin; PG-G, prostaglandin glycerol ester.

Atomic coordinates for LYPLA2-PMSF have been deposited in the Protein Data Bank (PDB) with accession number 6BJE.

[1]To whom correspondence should be addressed.
e-mail: larry.marnett@vanderbilt.edu

[S] The online version of this article (available at http://www.jlr.org) contains a supplement.

do so via respective receptor interactions. Regardless of mechanism, accumulated data suggest that LysoPLs play a significant role in modulating the phosphorylation state of the Ras/Raf/MEK (MAPK/ERK kinase)/ERK cascade (16, 18, 25–27). This signaling pathway is critical for the regulation of cell-cycle progression and differentiation (28–31). Indeed, LysoPL-mediated activation of the MAPK signaling pathway has consistently been shown to induce neuronal differentiation in neuroblastoma cells (16–19).

As LysoPLs are potent signaling molecules, their cellular levels are carefully regulated through three primary enzymatic pathways: lysophospholipase-mediated hydrolysis, acyltransferase-mediated generation of phospholipids (PLs), and transacylase-mediated generation of PLs. In mammalian cells, the lysophospholipase pathway predominates (32–38). Lysophospholipase A1 (LYPLA1) and lysophospholipase A2 (LYPLA2) are cytosolic serine hydrolases with esterase and thioesterase activity that are partially responsible for the metabolism of LysoPLs. LYPLAs hydrolyze LysoPLs at the sn-1 and, to a lesser extent, sn-2 positions to yield a FFA and a derivatized glycerophosphate that can then be recycled by a variety of phospholipases and acyltransferases to restructure the composition of the lipid membrane in a process called the Lands cycle (**Scheme 1**) (39–42). Inhibition of these regulatory mechanisms and the associated changes in LysoPL homeostasis have been associated with a variety of neurological diseases, including cerebral atherosclerosis, vascular dementia, and Alzheimer's disease (24, 43–47).

In addition to their role in the degradation of LysoPLs, LYPLAs display other activities. For example, the monoacylglycerol and endocannabinoid, 2-arachidonoylglycerol, is oxygenated by cyclooxygenase-2 to generate prostaglandin glycerol esters (PG-Gs) (48, 49). Our previous work has identified LYPLA2 as a PG-G hydrolase, converting PG-Gs to free prostaglandins (PGs) (41). This suggests a role for LYPLA2 in endocannabinoid metabolism. Furthermore, LYPLA1 and LYPLA2 are among a small pool of enzymes known to exhibit thioesterase activity on palmitoylated proteins such as the $G_{5\alpha}$ subunit of heterotrimeric G proteins and Ras (50–52). This posttranslational modification serves to alter protein conformation and/or tether a cytosolic protein to a lipid membrane with the addition of a lipophilic acyl moiety covalently bound to cysteine residues via a thioester linkage (53–56). LYPLA1 and LYPLA2 act to remove these acyl modifications as part of a dynamic palmitoylation process, regulating the subcellular location and conformation of a variety of cellular proteins (50, 52, 54, 57).

Despite relatively high sequence homology (68% identical, 83% similar), LYPLA1 and LYPLA2 display moderate substrate specificity in regard to LysoPL hydrolysis (32, 58–60). For example, whereas LYPLA1 displays general promiscuity in regard to the different LysoPL classes, LYPLA2 is considered more specific, preferring LPCs and LPEs. However, most of this work has been done with recombinant enzymes and exogenous substrate, despite the fact that substrate specificity of serine hydrolases differs between in vitro and cellular settings, where subcellular location, competitive metabolism, and protein expression levels impact relevant substrate availability (61).

To understand the substrate specificity of LYPLA1 and LYPLA2 in cells, we have utilized a murine Neuro2a neuroblastoma model, in which LYPLA activity is relatively high and commonly studied (62, 63). Using CRISPR-Cas9 technology, we have generated Neuro2a KO cell lines lacking *Lypla1*, *Lypla2*, or both genes to quantify and compare endogenous LysoPL levels in the absence of respective lysophospholipase activity. This approach offers a physiologically relevant model to determine the roles of LYPLA1 and LYPLA2 in LysoPL hydrolysis, as well as the consequences of the loss of their activity. Our results demonstrate that the roles played by the two enzymes in intact cells are not necessarily reflected by the results obtained with purified protein preparations.

MATERIALS AND METHODS

Chemicals, reagents, and statistics

All reagents were purchased from Sigma-Aldrich (St. Louis, MO), unless otherwise stated. PG-Gs and deuterated PGs (PGE_2-d_4)

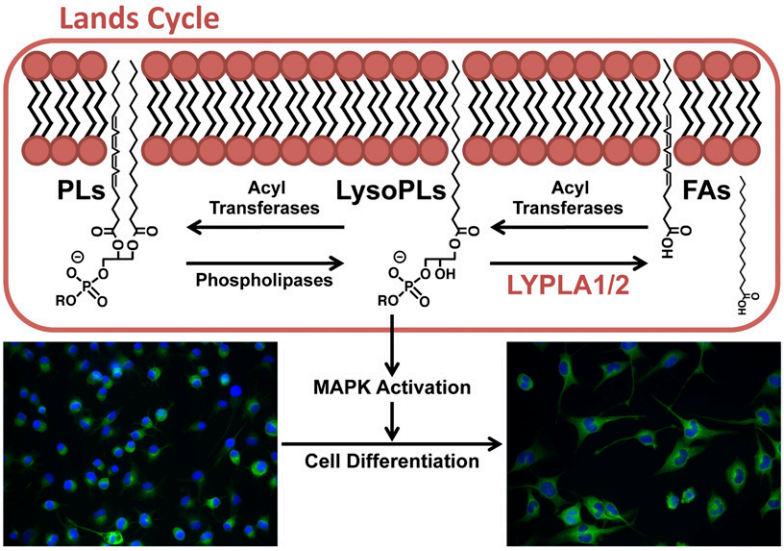

Scheme 1. The Lands cycle describes a PL remodeling pathway, demonstrating the interchangeability of acyl moieties and glycerophosphate headgroups by a variety of acyl transferases and phospholipases. Lysophospholipase activity by LYPLA1 and LYPLA2 removes the acyl moieties from various LysoPL species to modulate their potent signaling effects, such as MAPK activation and resultant cell differentiation.

were purchased from Cayman Chemicals (Ann Arbor, MI). All LysoPLs were purchased from Avanti Polar Lipids (Alabaster, AL). LC/MS solvents were from Fisher (Pittsburgh, PA). The 16:0-d_3 LPC was synthesized as described in supplemental data. Recombinant enzyme was expressed and purified as described previously, using cDNA from OriGene Technologies (Rockville, MD) (41). HIS-Select nickel affinity beads were from Sigma-Aldrich. HiPrep 16/60 Sephacryl S-200 HR was from GE Healthcare (Little Chalfont, UK). Neuro2a cells were obtained from the American Type Culture Collection (Manassas, VA). Cell culture reagents were purchased from Invitrogen (Grand Island, NY). All experiments were performed twice in triplicate, unless otherwise noted, and statistical significance was determined using one-way ANOVA, unless otherwise noted.

Cell culture

Neuro2a cells were maintained as adherent cultures in DMEM supplemented with 10% FBS from Atlas Biologicals (Fort Collins, CO). Cells were cultured at 37°C and 5% CO_2, grown to no more than 75% confluency, and trypsinized to passage.

X-ray crystallography

Recombinant human LYPLA2 (10 mg/ml) was preincubated with PMSF (10× molar ratio). Crystals were produced by hanging-drop vapor diffusion with drops containing 2 µl of enzyme-inhibitor complex and 2 µl of reservoir solution containing 0.1 M sodium citrate (pH 5.6) and 15–30% polyethylene glycol 3350. After 1∼2 weeks, irregular crystals formed and were supplemented with 25% glycol for cryopreservation. Diffraction data for LYPLA2-PMSF were collected on the Advanced Photon Source LS-CAT beamline 24-ID-E at 100 K. The data were processed with X-ray diffraction spectrometry and solved to 2.70 Å resolution by molecular replacement using Phaser with the A chain of LYPLA1 [Protein Data Bank (PDB) accession no. 1FJ2] as the search model. Two monomers were present in one asymmetric unit. Difference electron density maps contoured at 3σ showed the presence of a phenylmethylsulfonyl moiety associated with active Ser122. Data collection and refinement statistics for each structure are listed in supplemental Table S1. Figures were generated using PyMol Molecular Graphics system (Schrödinger). Atomic coordinates for LYPLA2-PMSF have been deposited in the PDB (accession no. 6BJE).

Recombinant LYPLA activity assays

Recombinant enzyme solutions (100 nM) were prepared in PBS with or without 0.5% (w/v) FA-free BSA, and 100 µl aliquots of each solution were preincubated at 37°C for 5 min. PGE_2-G, 16:0-d_3 LPC, or a mix of sn1- and sn2-18:0 LPC (1.5 nmol) was added in 1 µl ethanol, and samples were vortexed and then incubated at 37°C for 10 min. For quantitation of product formation (PGE_2-G and 16:0-d_3 LPC), enzymatic activity was quenched by adding 1 ml of ice-cold ethyl acetate with 0.5% (v/v) acetic acid containing either 20 ng PGE_2-d_4 or 1 nmol 16:0-d_{31} as internal standards. Samples were vortexed, and the organic layers were collected and dried under nitrogen. To quantify PG-G hydrolysis, extracts were resuspended in 200 µl acetonitrile and analyzed via LC/ESI/MS/MS, as described below. To quantify 16:0-d_3 LPC hydrolysis, samples were derivatized with pentafluorobenzyl (PFB) bromide based on a previously described method with minor adaptions (64). Specifically, extracts were reconstituted in 150 µl acetonitrile, and then 200 µl of 100 nM tetrabutylammonium hydrogen sulfate in 100 nM dibasic sodium phosphate buffer was added. Following addition of 200 µl 2% (v/v) PFB bromide in chloroform, the samples were vortexed and sonicated for 45 min at 35% output using a Virsonic Cell Disrupter (model 16-850), and then lipids were extracted via the addition of 1 ml of 9:1 hexanes:ethanol. The organic layer was removed, dried under nitrogen, and resuspended in 200 µl acetonitrile for analysis via LC/atmospheric-pressure chemical ionization (APCI)/MS/MS, as described below. For quantitation of substrate remaining (18:0 LPC), enzymatic activity was quenched by adding 100 µl of ice-cold ethanol with 0.5% (v/v) acetic acid containing 2 µM 17:0 LPC as an internal standard. Samples were immediately analyzed via LC/ESI/MS/MS, as described below, to prevent the equilibration of sn1-18:0 and sn2-18:0 LPC isomers via acyl migration.

Generation and validation of LYPLA KO cells using CRISPR-Cas9

CRISPR technology was utilized to generate genetic LO cells as described by Ran et al. (65). gRNAs were designed to target early exons of the LYPLA1 and LYPLA2 genes. gRNA oligomers (LYPLA1 gRNA: TCCGATGCCCGCCGTTGTGC; LYPLA2 gRNA: AGCTGAGCGGGAAACGGCCG) were annealed, phosphorylated, and ligated into digested pspCas9(BB)-2A-puro plasmid (plasmid no. 62988, Addgene, Cambridge, MA). Neuro2a cells (1.5×10^5) were suspended in 2 ml of DMEM supplemented with 10% FBS and plated in 6-well plates. The following day, 5 µg of each plasmid was combined with 10 µl Lipofectamine 2000 reagent (Invitrogen) in 1 ml Opti-MEM and incubated at room temperature for 30 min. Neuro2a culture medium was replaced with the appropriate plasmid-lipofectamine solution, and cells were incubated at 37°C for 24 h. The medium was then replaced with fresh DMEM plus 10% FBS, and cells were allowed to recover for 24 h at 37°C prior to the addition of 0.75 µg/ml puromycin. Cells were incubated at 37°C for 48 h before replacing the medium. After recovering for ∼1–2 weeks, cells were pelleted, resuspended in sorting buffer (PBS + 4% FBS), and strained to separate clumps of cells. Solutions were sorted by flow cytometry using a 5-laser BD LSRII with a 100 µm nozzle at the Vanderbilt Medical Center Flow Cytometry Core to isolate single cell cultures in 96-well plates for each cell line. Clones were incubated until they reached ∼70% confluency and then passaged until enough cells could be harvested for KO validation via Western blotting. Cells lacking both *Lypla1* and *Lypla2* genes, or double-KO (DKO) cells, were generated by repeating this process to target the *Lypla1* gene in the *Lypla2*$^{-/-}$ cells.

Western blot analysis

Protein expression was determined by Western blot analysis as previously described (41, 66). Samples were separated by SDS-PAGE. Then, proteins were transferred to a nitrocellulose membrane and blocked with Odyssey Blocking Buffer (LI-COR, Lincoln, NE) for 1 h at room temperature and probed with rabbit anti-LYPLA1 (1:1,000 v/v, abcam, Cambridge, UK), rabbit anti-LYPLA2 (1:1,000 v/v, Vanderbilt Antibody and Protein Resource Core; polyclonal rabbit anti-LYPLA2 antibody was generated by the Vanderbilt Antibody and Protein Resource Core and can be obtained through contact with corresponding author, L. J. Marnett.), rabbit anti-ERK1/2 [1:1,000 v/v, Cell Signaling Technologies (CST), Danvers, MA], rabbit anti-phospho-ERK1/2 (1:1,000 v/v, CST), rabbit anti-MEK1/2 (1:1,000 v/v, CST), rabbit anti-phospho-MEK1/2 (1:1,000 v/v, CST), or goat anti-β-actin (1:5,000 v/v, Santa Cruz Biotechnologies, Santa Cruz, CA) overnight at 4°C. Membranes were washed and incubated with IR-visible anti-rabbit or anti-goat secondary Abs (1:5,000 v/v, LI-COR). Blots were visualized using an Odyssey IR Imager.

Assay for LYPLA activity in cell lysates

WT, *Lypla1*$^{-/-}$, *Lypla2*$^{-/-}$, or DKO cells (1×10^6) were plated in 8 ml DMEM with 10% FBS in 100 mm plates and incubated at 37°C for 24 h prior to harvesting. Cell pellets were suspended in a buffer containing 25 mM Tris (pH 7.5), 0.1 mM EDTA, and 0.1 mM DTT. Cells were sonicated into solution via 10 × 1 s pulses

at 35% output. Debris was pelleted via centrifugation at 15,000 *g* for 10 min, and soluble protein concentration in the supernatant was determined via Pierce™ BCA protein assay (Thermo Scientific, Rockford, IL). Solutions (250 μg/ml) of each enzyme were prepared, and 100 μl aliquots were preincubated at 37°C for 5 min. PGE_2-G or 16:0-d_3 LPC (1.5 nmol) was added in 1 μl ethanol, and samples were vortexed and incubated at 37°C for 1 h. Enzymatic activity was quenched by adding 1 ml of ice-cold ethyl acetate with 0.5% (v/v) acetic acid containing either 20 ng PGE_2-d_4 or 1 nmol 16:0-d_{31} as internal standards. Samples were vortexed, and organic layers were collected and dried under nitrogen. FAs were derivatized as described above, and LC/MS/MS analysis was then performed as described below.

LysoPL extraction

WT, *Lypla1*$^{-/-}$, *Lypla2*$^{-/-}$, or DKO cells (1×10^6) were plated in 8 ml DMEM with 10% FBS in 100 mm plates and incubated at 37°C for 24 h. Cells were then scraped into 3 ml ice-cold PBS and pelleted. LysoPLs were extracted from cell pellets using a method adapted from Zhao and Xu (67), by resuspending in 200 μl of ice-cold methanol containing 50 nM 17:0 LPA, 250 nM 17:0 LPC, 50 nM 17:1 LPE, 50 nM 17:1 LPG, 50 nM 17:1 LPI, and 150 nM 17:1 LPS. Cells were sonicated with 10 × 10 s pulses at 35% output, and protein was pelleted. Methanol extracts were collected for lipid analyses via LC/ESI/MS/MS as described below. Protein pellets were resuspended in 1 ml PBS containing 0.2% SDS, sonicated with 10 × 10 s pulses at 35% output, and subjected to BCA assay to quantify input protein.

LC/MS/MS analysis

For activity assays, samples were run on an LC/MS system consisting of a Shimadzu liquid chromatograph in line with a SCIEX 3200 QTrap mass spectrometer. Analyst software (version 1.6.2) was used for instrument control, data acquisition, and data processing. Quantitation was achieved via stable isotope dilution against the indicated internal standard of PGE_2-d_4 or 16:0-d_{31}. For PGE_2 analysis, reconstituted samples were run in negative mode on a system configured as described in supplemental Table S2A, B. For 16:0-d_3 analysis, reconstituted samples were run in negative mode on a system configured as described in supplemental Table S3A, B. The Luna liquid chromatography reverse-phase C18 columns were from Phenomenex (Torrance, CA).

For lipidomics experiments, samples were run on an LC/MS system consisting of a Shimadzu liquid chromatograph in line with a SCIEX 3200 QTrap or a SCIEX 6500 QTrap mass spectrometer based on methods described by Okudaira et al. (68) and Aaltonen et al. (69). This method isolates LysoPLs from other glycerolipid and glycerophospholipid species. Analyst software (version 1.6.2) was used for instrument control, data acquisition, and data processing. Quantitation was achieved via internal standard dilution against the respective unnatural 17:0 or 17:1 LysoPL depending on the class being investigated. In all cases, the mass spectrometer was configured in electrospray mode and operated in multiple reaction monitoring mode. LPC species were analyzed in positive-ion mode with LC parameters described in supplemental Table S4A. LPE, LPS, LPG, LPA, and LPI species were analyzed in negative-ion mode with LC parameters described in supplemental Table S4B. Fragmentation patterns of all LysoPL species are described in supplemental Table S4C.

Immunocytochemistry

WT, *Lypla1*$^{-/-}$, *Lypla2*$^{-/-}$, or DKO Neuro2a cells (4×10^3) were plated in 100 μl DMEM with 10% FBS in a 96-well plate. After 48 h, the medium was replaced with 100 μl DMEM containing 2% FBS [established conditions for inducing neuronal differentiation (17, 70–72)] and either 2.5 μM retinoic acid, 10 μM PD98059 [an inhibitor of MEK activation used to study neuronal differentiation (73)], 10 μM 16:0 LPA, 10 μM 16:0 LPC, or DMSO control. Cells were cultured for 48 h to promote differentiation, based on a method adapted from Riboni et al. (74). Cells were then washed 2× with 100 μl PBS and fixed with the addition of 3.7% formaldehyde in PBS, followed by shaking at room temperature for 20 min. Cells were then washed 2× with PBS and permeabilized with 0.15% Triton X-100 in PBS for 10 min at room temperature. Cells were again washed 2× with PBS and blocked with Odyssey Blocking Buffer by shaking for 1 h at room temperature. Cells were then stained with mouse anti-βIII-tubulin (1:2,000 v/v, abcam) for 24 h at 4°C while shaking. The following day, cells were washed 3× with TBS containing 0.1% (v/v) Tween (TBS-T) for 10 min while shaking at room temperature, prior to the addition of AlexaFluor 488-conjugated donkey anti-mouse Ab (1:1,000 v/v, Life Technologies, Carlsbad, CA) and DAPI (1:1,000 v/v, Invitrogen) for 1 h while shaking at room temperature. Cells were then washed again 3× with TBS-T and rinsed 3× with PBS. Stained cells were imaged at 10× power in a 5 × 5 array, and the data were processed using a MetaXpress Micro XL automated microscope imager, which generated a single composite image per well. Neurite outgrowth quantification was performed using the following parameters: minimum neuron area = 120 μm^2, maximum neuron width = 27 μm, minimum neuron intensity above background = 500 gray levels, minimum nuclear width = 5 μm, maximum nuclear width = 14 μm, minimum nucleus intensity above background = 3,000 gray levels, maximum neurite outgrowth width = 4 μm, minimum neurite outgrowth length = 10 μm, and minimum neurite outgrowth intensity above background = 200 gray levels.

RESULTS

LYPLA1 and LYPLA2 display high structural alignment

The crystal structure of apo-LYPLA1 (PDB accession no. 1FJ2) suggests that the enzyme is unusual in that it lacks the traditional cap domain found in other members of the α/β-hydrolase superfamily (75). Instead, the β4-α2 loops are positioned as a flexible lid covering the active-site serine, creating a potential hydrophobic channel for lipid binding. Another crystal structure of LYPLA1 (PDB accession no. 5SYM) and the structure of LYPLA2 (PDB accession no. 5SYN) have recently been solved with the specific inhibitors, ML348 and ML349, respectively, bound in their active sites (76). Although the previously reported structures of LYPLA1 and LYPLA2 suggest the proteins form weak dimers, size-exclusion chromatography indicates that both enzymes are active as monomers (data not shown).

We used sparse matrix screening of crystallization to obtain the crystals that were used to solve the structure of LYPLA2 covalently modified by the general serine hydrolase inhibitor, PMSF, at 2.7 Å resolution (PDB accession no. 6BJE) (**Fig. 1**, supplemental Table S1). This is the second structure of LYPLA2 to be reported, and the first with a covalent modification of the active site Ser122. Consistent with the previously reported structure, LYPLA2-PMSF crystallized as a dimer, although it is equally active in monomer and dimer conformations. Crystals of apo-LYPLA2 were also obtained but failed to diffract for structure studies due to lattice defects. The data confirm that, like LYPLA1, LYPLA2 lacks a cap domain, which is replaced by the β4-α2 loops (highlighted in blue in Fig. 1) that act as a flexible lid

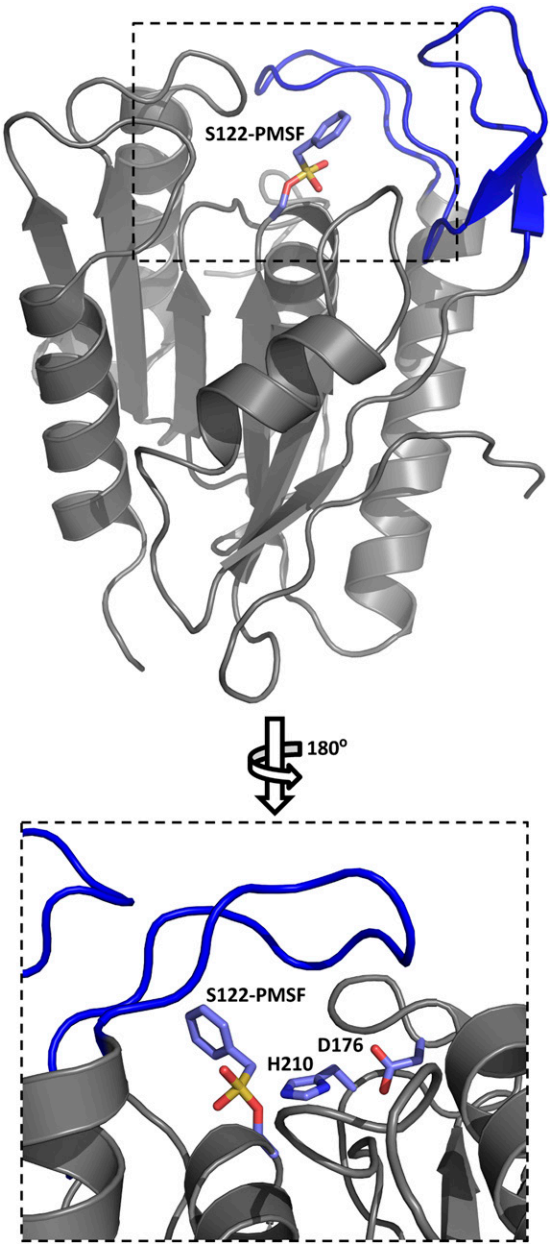

Fig. 1. Crystal structure of LYPLA2-PMSF (PDB accession no. 6BJE) shown in cartoon representation with orientation exposing active Ser122 with PMSF modification. *B5-α2* loop enveloping the active site is highlighted in blue. Catalytic triad, Asp176, His210, and active Ser122, is shown in close-up view, rotated 180°. X-ray data collection and refinement statistics are described in supplemental Table S1.

near the active site. The LYPLA2-PMSF structure is very similar to that of LYPLA2-ML349; however, small differences in conformation are noted. For example, the β5-α2 loop in the two structures is present in distinct conformations (supplemental Fig. S1), with the LYPLA2-ML349 loop extended slightly further than that of LYPLA2-PMSF. This suggests that the loop is able to move to accommodate substrates or inhibitors binding in the channel adjacent to the active Ser122. Additionally, the modified Ser122-PMSF demonstrates a slight shift in position compared with the unmodified Ser122 of the LYPLA2-ML349 structure, likely due to the steric bulk of the PMSF modification.

Consistent with the relatively high sequence homology of LYPLA1 and LYPLA2 (**Fig. 2A**), a least-squares comparison of their coordinates reveals that the two proteins are folded in nearly identical conformations (Fig. 2B). Superposition across all 215 aligned residues yielded a root-mean-square deviation (RMSD) of 0.878 Å and a quality of alignment (Q-score) of 0.838, suggesting that the protein structures differ by no more than 1 Å (77). This high degree of sequence and structural similarity suggests that the two proteins may share significant overlap in substrate specificity and hydrolytic activity.

LYPLA1 is a PG-G hydrolase in vitro

A recent report from our laboratory identified LYPLA2 as the major PG-G hydrolase in cancer cells. At that time, LYPLA1 was ruled out on the basis of siRNA knockdown in cells, but the enzyme's PG-G hydrolytic activity was not evaluated directly in vitro with purified recombinant protein (41). Therefore, we quantified both LYPLA1 and LYPLA2 activity toward a representative PG-G substrate, PGE_2-G. Additionally, as both LYPLA1 and LYPLA2 have been shown to robustly hydrolyze 16:0-LPC, we quantified hydrolytic activity toward the 16:0-LPC species as a representative LysoPL substrate. However, as the product of LysoPL hydrolysis by LYPLAs is a glycerophosphate headgroup (too small and polar for LC separation) and a FA [notoriously omnipresent in solvents, plastics, and glassware, as well as difficult to ionize and fragment (78–80)] (**Fig. 3A**), we utilized an isotopically labeled 16:0-d_3 LPC species and a PFB-Br derivatization for these assays (64). The derivatization yields a PFB-esterified acyl chain, which has electron-capturing properties to enable sensitive ionization and detection in APCI/MS/MS. This method allowed for the LC/MS/MS-based quantification of a FA species by avoiding contamination and ionization issues.

As demonstrated in Fig. 3B, both enzymes were able to hydrolyze these substrates. LYPLA1 hydrolyzed PGE_2-G at a rate of 48.1 ± 0.5 μmol/min/mg compared with 93.3 ± 4.7 μmol/min/mg for LYPLA2, and LYPLA1 hydrolyzed 16:0-d_3 LPC at a rate of 127 ± 8 μmol/min/mg compared with 129 ± 9 μmol/min/mg for LYPLA2. Thus, contrary to our findings in intact cancer cells, recombinant LYPLA1 displayed substantial PG-G hydrolytic activity. However, whereas the two enzymes hydrolyzed 16:0-d_3 LPC with equivalent specific activity, LYPLA2 was significantly more active than LYPLA1 toward PGE_2-G. It has been reported that BSA is able to improve hydrolysis of lipid substrates in recombinant serine hydrolase activity assays, presumably by acting as a lipid carrier to better mimic the conditions of a cellular setting, and we have recently shown that the presence of BSA has a significant effect on LYPLA2-mediated PG-G hydrolysis (41, 81). Therefore, we also added BSA to the enzyme solutions to promote substrate availability and compared enzymatic activity toward both PG-G and LysoPL substrates. In the presence of BSA, LYPLA1 hydrolyzed PGE_2-G at a rate of 64.2 ± 1.7 μmol/min/mg compared with 170 ± 8 μmol/min/mg for LYPLA2, and LYPLA1 hydrolyzed 16:0-d_3 LPC at a rate of 137 ± 14 μmol/min/mg compared with 137 ± 2 μmol/min/mg for LYPLA2. These

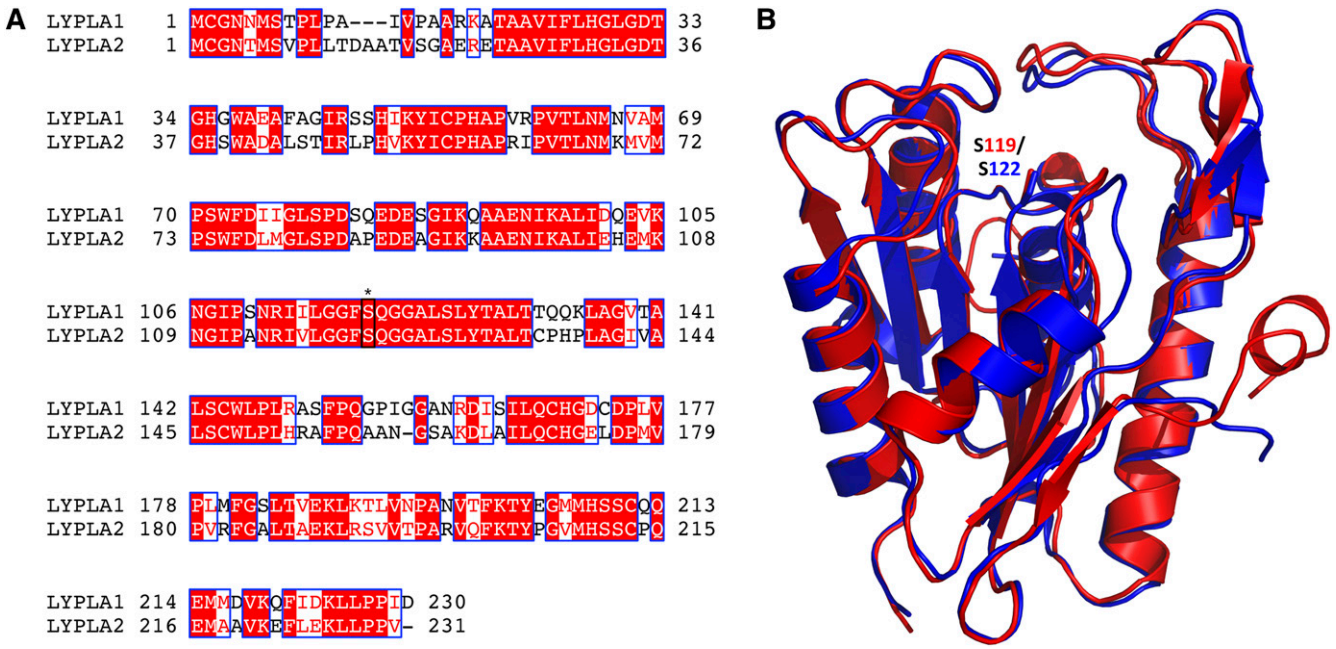

Fig. 2. Comparison of sequences and structures of LYPLA1 and LYPLA2. A: Sequence alignment of LYPLA1 and LYPLA2, with identical residues designated by white text highlighted in red, similar residues designated by red text, and similar sequences designated by blue boxes. The catalytic Ser119 and Ser122 of LYPLA1 and LYPLA2, respectively, are marked with a black box and a *. B: Structural alignment of LYPLA1 (PDB accession no. 1FJ2), shown in red, and LYPLA2, shown in blue, suggests a high degree of structural similarity between the proteins. Active Ser residues are labeled S119 in red and S122 in blue in LYPLA1 and LYPLA2, respectively. RMSD = 0.878 Å; Q-score = 0.838.

results suggest that the addition of BSA promotes the hydrolytic activity of LYPLA2 but not LYPLA1 toward PG-Gs, without significantly affecting the activity of either enzyme toward LysoPLs.

Preliminary studies by our lab have suggested that LYPLA2 prefers the sn1-isomer of PG-G and glycerolipids (41). To determine substrate specificity of LYPLAs toward sn1- versus sn2-isomers of LysoPLs, equilibrium mixtures of sn1-18:0 LPC (~80%) and sn2-18:0 LPC (~20%) were added to 100 nM enzyme solutions of LYPLA1, LYPLA2, or a no enzyme control under conditions in which hydrolysis occurred faster than isomeric equilibration. The isomeric composition of the remaining 18:0 LPC substrate was assessed immediately after quenching with acidified ethanol to prevent acyl migration, and PBS controls were included to ensure that changes to isomeric composition were not merely a result of isomeric equilibration. With both LYPLA1 and LYPLA2, only sn1-18:0 LPC isomer levels were significantly decreased after 10 min compared with those in the PBS controls (Fig. 3C). These data demonstrate the specificity of LYPLAs toward sn1-LysoPLs, which is consistent with our published activity of LYPLA2 toward 1(3)-PG-Gs and 1(3)-arachidonoylglycerol.

KO of *Lypla* genes results in decreased hydrolytic activity

As our results suggested that in vitro enzymatic activity does not necessarily reflect the metabolic contribution of that enzyme in vivo, we sought to better understand the role of LYPLA1 and LYPLA2 in LysoPL turnover in intact cells. CRISPR-Cas9 technology was utilized to generate stable genetic KOs of *Lypla1*, *Lypla2*, or both genes in murine Neuro2a neuroblastoma cells. Sanger sequencing was used to verify genetic editing at sites in the *Lypla* genes targeted by respective gRNAs and overexpressed Cas9 protein. Genetic KOs were validated at the protein level using Western blotting with Abs directed toward LYPLA1 and LYPLA2 (**Fig. 4A**). Notably, the level of each LYPLA was unaffected by KO of the other isoform. The ability of the cell lines to hydrolyze the canonical PG-G and LysoPL substrates of the LYPLAs was tested using cellular lysates and the previously described hydrolytic activity assays. In addition to avoiding palmitic acid contamination from plastics and solvents, the use of isotopically labeled 16:0-d_3 LPC in this assay was instrumental to avoid mistaking the endogenous palmitic acid present in cells for hydrolyzed product of the exogenous substrate. This same problem did not arise in the case of PG-G hydrolysis, as Neuro2a cells lack the cyclooxygenase activity required to generate endogenous PG-Gs or PGs. Enzymatic activity of Neuro2a lysates that had been normalized for protein concentration was quantified as the percent of each substrate hydrolyzed as described in Fig. 3A. The percentages of PGE_2-G hydrolyzed in WT, *Lypla1*$^{-/-}$, *Lypla2*$^{-/-}$, and DKO cell lysates were 50.4 ± 1.3%, 51.3 ± 0.9%, 43.0 ± 0.6%, and 32.1 ± 0.4%, respectively, whereas the percentages of 16:0-d_3 LPC hydrolyzed in WT, *Lypla1*$^{-/-}$, *Lypla2*$^{-/-}$, and DKO cell lysates were 24.2 ± 3.3%, 23.4 ± 3.5%, 18.8 ± 0.7%, and 11.2 ± 0.3%, respectively (Fig. 4B). Similar to what we observed in our previous work using human cancer cell lines, *Lypla1*$^{-/-}$ cells exhibited the same PG-G hydrolytic activity as WT cells, whereas the activity in *Lypla2*$^{-/-}$ cells was significantly lower than that of WT cells. In DKO cells, PG-G hydrolysis was further decreased, suggesting that both enzymes contribute to PG-G hydrolysis and that LYPLA2 can better compensate

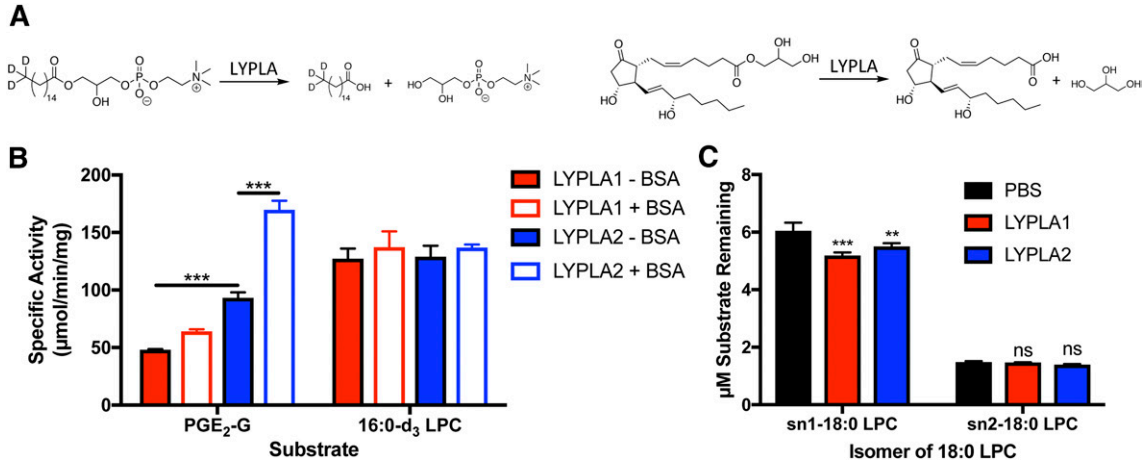

Fig. 3. Comparison of the activities of recombinant LYPLA1 and LYPLA2. A: Scheme of hydrolysis of 16:0-d_3 LPC (left) and PGE_2-G (right) by LYPLAs. B: Activity of recombinant LYPLA1 and LYPLA2 toward representative substrates PGE_2-G and 16:0-d_3 LPC with or without 0.5% (w/v) BSA. C: Activity of recombinant LYPLA1 and LYPLA2 toward sn1 and sn2 isomers of 18:0 LPC [1(3)-18:0 LPC and 2-18:0 LPC, respectively]. Data are expressed as micromolar substrate remaining after incubating in no enzyme control (PBS) or with LYPLA1 or LYPLA2. ** $P < 0.01$; *** $P < 0.001$. ns, not significant.

for loss of LYPLA1 than vice versa. This same trend is observed with LysoPL hydrolysis. Notably, however, DKO cells retained 64% and 46% of the PGE_2-G and 16:0-d_3 LPC hydrolytic activity of WT cells, respectively, indicating that other enzymes are available to catalyze both reactions. It is not possible to know whether expression of these enzymes increases to compensate for the loss of LYPLA1 and/or LYPLA2 in the KO cells. If so, these results would underestimate the contribution of the LYPLAs to PGE_2-G and 16:0-d_3 LPC hydrolysis in the WT cells.

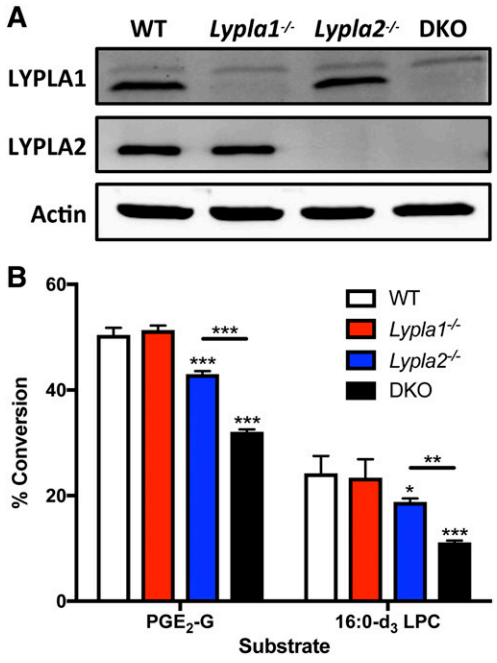

Fig. 4. Validation of *Lypla1*$^{-/-}$, *Lypla2*$^{-/-}$, and DKO Neuro2a cells. A: Western blot analysis of LYPLA1 and LYPLA2 in WT, *Lypla1*$^{-/-}$, *Lypla2*$^{-/-}$, or DKO cells. B: Hydrolytic activity of WT, *Lypla1*$^{-/-}$, *Lypla2*$^{-/-}$, or DKO cell lysates toward representative PGG and lysoPL substrates; data are shown as percent conversion of exogenous substrate to respective hydrolysis products. * $P < 0.05$; ** $P < 0.01$; *** $P < 0.001$.

LysoPL species are increased in DKO cells

With the decreased hydrolytic activity observed in the *Lypla* KO cells, we hypothesized that basal levels of LYPLA substrates would be consequentially increased. To test this hypothesis, we utilized an LC/MS/MS-based targeted lipidomics approach to quantify LPA, LPC, LPE, LPG, LPI, and LPS substrates containing the following acyl moieties at both the sn-1 and sn-2 positions of the glyceryl backbone: 16:0, 16:1, 18:0, 18:1, 18:2, 18:3, 20:4, 20:5, and 22:6. Absolute quantification of each lipid species was normalized to the amount of protein in each sample. As the variance of the LysoPL species was unequal between samples, and values in each sample were not normally distributed, one-way ANOVA could not be used to determine statistical significance. Instead, samples with normal distributions (skewness between −1 and 1) were analyzed by Welch's *t*-test, and samples with abnormal distributions (skewness less than −1 or greater than 1) were analyzed by the Wilcoxon rank-sum test. Statistically significant differences in LysoPL levels in *Lypla1*$^{-/-}$, *Lypla2*$^{-/-}$, or DKO cells were compared individually to those of WT cells. Results for every identified LysoPL species are listed in **Table 1**, with values that are significantly different from those of WT cells marked by boldface text. Additionally, these values are displayed in **Fig. 5A**–F as absolute quantities and in Fig. 5G–L as fold changes normalized to the LysoPL levels in WT cells (with WT values set to 1, represented by dotted lines).

As expected, LPCs were the most abundant of the LysoPL classes, with more prevalent species found in quantities near 500 pmol/mg protein. LysoPLs containing saturated acyl chains of 16 and 18 carbons were generally found at levels much higher than those containing longer or more unsaturated acyl chains. Whereas the LysoPL concentrations of *Lypla1*$^{-/-}$ cells were mostly comparable to those of WT cells [with the exception of 20:4 LPA (1.6-fold

TABLE 1. Basal LysoPL levels (pmol/mg protein) in WT, *Lypla1*$^{-/-}$, *Lypla2*$^{-/-}$, and DKO cells, presented as mean (SD)

Lipid species		Cell line							
		WT		*Lypla1*$^{-/-}$		*Lypla2*$^{-/-}$		DKO	
LPA	16:0	6.90	(3.15)	6.95	(1.82)	9.28	(1.84)	**16.2**	**(6.23)**
	16:1	3.23	(0.74)	4.23	(1.05)	3.31	(0.53)	**4.55**	**(1.18)**
	18:0	3.54	(0.92)	3.24	(0.96)	5.85	(2.84)	16.3	(14.0)
	18:1	4.35	(1.49)	4.85	(0.78)	6.08	(2.02)	8.97	(6.54)
	20:4	0.86	(0.11)	**1.38**	**(0.24)**	1.02	(0.34)	**1.36**	**(0.29)**
LPC	16:0	545	(86.6)	509	(41.8)	**823**	**(77.1)**	**1890**	**(713)**
	16:1	62.9	(8.52)	62.5	(6.70)	**85.0**	**(6.32)**	**243**	**(101)**
	18:0	464	(83.9)	442	(48.6)	549	(48.9)	**1410**	**(527)**
	18:1	416	(98.5)	460	(34.4)	498	(58.0)	**1220**	**(503)**
	18:2	25.1	(4.48)	26.8	(1.86)	**38.6**	**(2.63)**	**154**	**(66.4)**
	18:3	1.61	(0.30)	1.59	(0.12)	**2.91**	**(0.27)**	**9.81**	**(2.16)**
	20:4	41.4	(10.1)	**53.5**	**(6.34)**	51.4	(13.3)	**255**	**(167)**
	20:5	1.76	(0.46)	2.14	(0.76)	**3.88**	**(0.61)**	**16.4**	**(7.96)**
	22:6	23.3	(3.65)	23.7	(3.19)	24.8	(6.19)	**101**	**(61.5)**
LPE	16:0	30.4	(8.19)	25.7	(6.79)	35.8	(10.5)	**119**	**(74.3)**
	18:0	91.0	(44.0)	70.2	(24.6)	93.0	(40.4)	**299**	**(215)**
	18:1	63.3	(15.3)	53.9	(12.3)	50.0	(13.2)	**155**	**(106)**
	18:2	4.23	(1.78)	3.42	(0.99)	3.10	(1.51)	12.3	(9.95)
	20:4	25.2	(13.4)	26.8	(11.2)	21.1	(12.5)	94.5	(88.9)
	20:5	1.29	(0.06)	1.09	(0.16)	1.31	(0.36)	**2.31**	**(0.17)**
LPG	16:0	5.04	(0.38)	**3.99**	**(0.36)**	**6.00**	**(0.66)**	**13.8**	**(2.93)**
	18:0	4.18	(1.21)	3.01	(0.37)	5.08	(0.63)	**11.0**	**(2.42)**
	18:1	50.5	(2.44)	**31.9**	**(4.00)**	**29.0**	**(4.40)**	50.5	(14.4)
	20:4	0.24	(0.01)	0.32	(0.08)	0.23	(0.01)	**0.37**	**(0.01)**
LPI	16:0	15.4	(2.63)	10.8	(3.26)	**34.2**	**(6.33)**	**86.1**	**(33.3)**
	18:0	169	(44.2)	166	(119)	**254**	**(82.1)**	**572**	**(242)**
	18:1	96.7	(19.3)	88.6	(21.9)	**139**	**(15.6)**	**255**	**(101)**
	18:2	2.60	(0.43)	2.57	(0.44)	3.34	(0.71)	**8.63**	**(4.27)**
	20:4	9.07	(3.27)	11.1	(2.57)	10.5	(2.43)	**31.2**	**(22.9)**
LPS	16:0	5.80	(0.76)	5.65	(0.93)	5.52	(0.44)	**11.5**	**(3.73)**
	18:0	34.7	(5.69)	29.9	(4.60)	34.4	(8.78)	**80.0**	**(43.7)**
	18:1	15.3	(1.65)	19.4	(5.31)	**26.3**	**(6.55)**	**91.0**	**(72.9)**
	20:4	0.62	(0.03)	0.61	(0.06)	0.60	(0.08)	**1.05**	**(0.13)**

Boldface values indicate $P < 0.05$, determined by Welch's *t*-test or the Wilcoxon rank-sum test for samples with normal or abnormal distributions, respectively.

increase) and 20:4 LPC (1.3-fold increase)], *Lypla2*$^{-/-}$ cells displayed some significant differences from WT cells in certain LysoPL species, such as 16:0 LPC (1.5-fold increase), 18:2 LPC (1.5-fold increase), 18:3 LPC (1.8-fold increase), 16:0 LPI (2.2-fold increase), and 18:0 LPI (1.5-fold increase). However, any differences in the single-KO cells were overshadowed by the much greater increases in the levels of many LysoPLs in the DKO cells. This is especially notable with the LPCs, LPEs, LPIs, and LPSs, of which most lipid species increased by 3- to 9-fold in the DKO relative to the WT cells. These results are consistent with the lysophospholipase activity measured in cell lysates (Fig. 4B). Notably, although these large changes in LysoPLs were observed, FA levels in the lipid extracts were quantified via PFB-derivatization, as described above, and no significant differences were seen in the KO cells (supplemental Fig. S4). This is not surprising, as cellular LysoPL levels are roughly 1,000-fold lower than those of FFAs; therefore, LysoPL-hydrolysis is unlikely to be a major contributor to the levels of cellular FAs. Together, the data suggest that LYPLA2 makes a greater contribution to LysoPL hydrolysis than LYPLA1 and/or can fully compensate for the loss of LYPLA1. However, the loss of both enzymes appears to unmask a role for LYPLA1 that is not revealed by the single-KO cells.

Interestingly, although lipids in each of the LysoPL classes exhibited significant increases in the DKO cells, albeit at varying magnitudes, there was no consistent pattern in the exact species (as designated by the acyl chain) most affected. This suggests that LYPLA substrate specificity is more dependent on LysoPL class than acyl chain identity, with LPC, LPE, and LPI species in the DKO cells increasing by >300% on average compared with WT cells. Furthermore, in contrast to in vitro studies where LYPLA2 has been shown to prefer fully saturated LysoPL substrates, unsaturated LysoPLs of each class in the DKO cells are significantly increased, especially in the LPC, LPE, and LPI classes (41). Indeed, the highest fold changes between DKO and WT cells occurred in the polyunsaturated LPCs, although these were mostly minor species. Of course, it is possible that neither LYPLA1 nor LYPLA2 plays a direct role in changing some LysoPL levels. It is possible that genetic deletions of multiple lipases involved in the Lands cycle alter lipid-remodeling pathways, leading to indirect increases of specific LysoPL species that may not necessarily be directly hydrolyzed by either enzyme. Such remodeling might also occur through the compensatory overexpression of other enzymes in response to the deletion. Nevertheless, these data demonstrate that the in vivo impact of a specific serine hydrolase cannot be easily predicted by in vitro studies of its substrate selectivity, stressing the importance of cellular models in studying enzymatic activity.

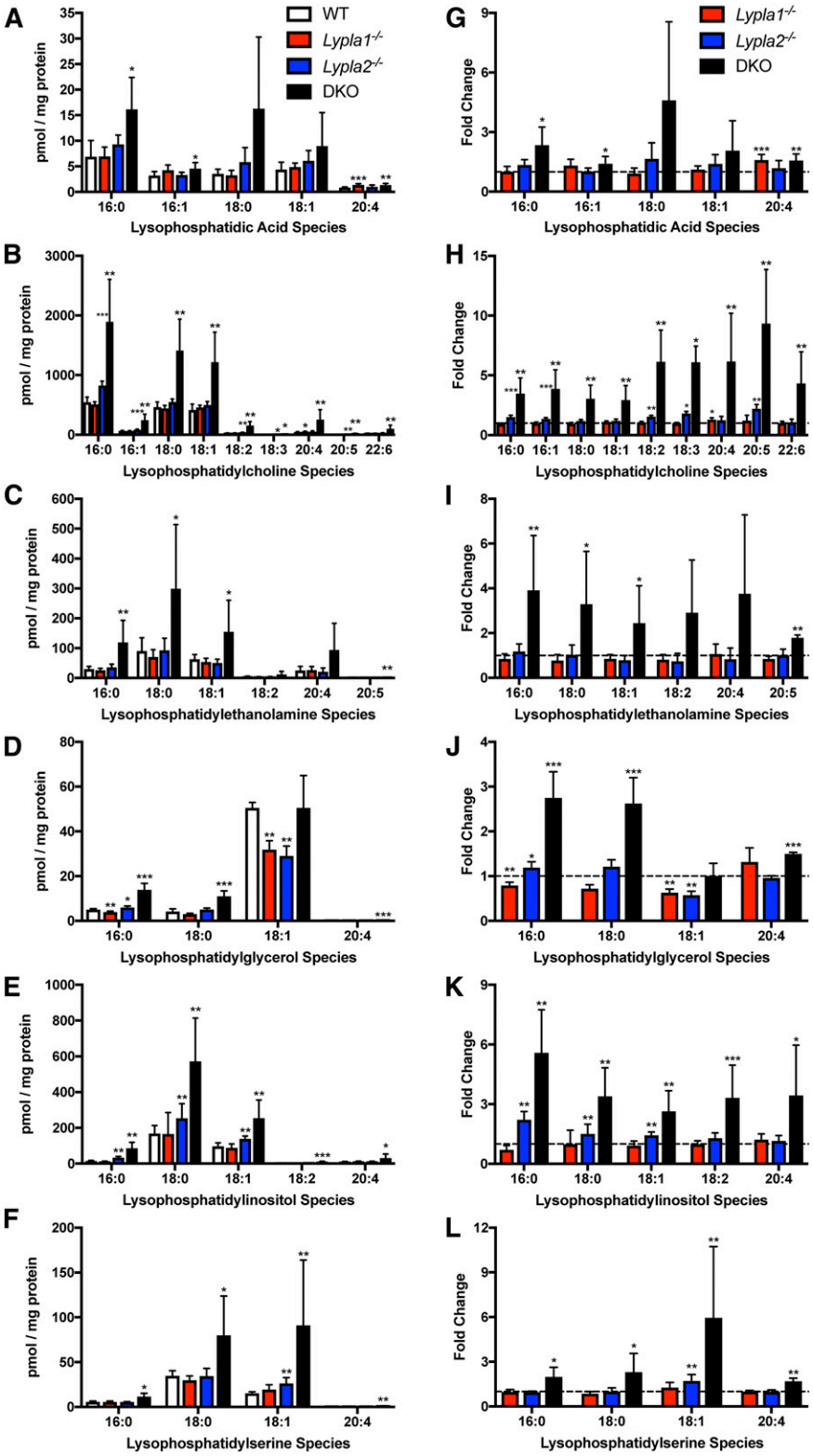

Fig. 5. LysoPL quantification via LC/MS/MS in methanol extracts of WT, *Lypla1*$^{-/-}$, *Lypla2*$^{-/-}$, and DKO Neuro2a cells. Each lipid class was quantified using an exogenous 17-carbon length LPL internal standard and normalized to total protein content. A–F: Data represented as pmol LysoPL/mg protein. G–L: Data represented as fold changes normalized to WT values. *$P < 0.05$; **$P < 0.01$; ***$P < 0.001$, determined by Welch's *t*-test or the Wilcoxon rank-sum test for samples with normal or abnormal distributions, respectively.

LysoPL signaling pathways are overactive in DKO cells

The above data indicated that *Lypla* KO leads to increases in LysoPLs, which are well-characterized signaling molecules. As activation of the MAPK pathway is commonly associated with LysoPL signaling, we evaluated the phosphorylation states of individual kinases within the MAPK cascade using

phospho-specific Abs and compared them between WT and *Lypla* KO cells. When normalized to total MEK1/2, phosphorylated MEK1/2 was significantly higher in DKO than WT or either single-KO cell lines (**Fig. 6A**). Additionally, when normalized to total ERK1/2, phosphorylated ERK1/2 demonstrated this same trend with significant increases observed in DKO cells (Fig. 6B). The increased phosphorylation states of these proteins suggest that the elevated LysoPLs in DKO cells are activating the MAPK signaling pathway.

Neuronal differentiation is increased in LYPLA KO cells

The consequences of ERK phosphorylation have been extensively studied and are dependent on cell type. In neuroblastoma cells, the MAPK signaling pathway is known to induce neuronal differentiation, increasing neurite outgrowth and cell area and initiating gap junction intracellular communication (16–19). To assess the impact of MAPK signaling pathway activation in the context of LYPLA deficiency, we utilized immunocytochemistry and high-throughput imaging to compare the morphology and degree of neuronal differentiation between the WT and *Lypla* KO Neuro2a cells. Retinoic acid was also used as a positive control to induce differentiation in WT cells. After fixing and permeabilizing the cells in 96-well plates, the overall shape of each cell was visualized using an Ab directed toward βIII-tubulin (green). Each cell was identified using the nuclear stain DAPI to enable cell counting and normalization between samples (**Fig. 7A**). Multiple 10× magnification images were "stitched together" to create one composite image for each well (one replicate), and the images were processed with MetaXpress software using the neurite outgrowth application. This technology allowed us to take large-scale images of entire cell populations in 96-well plates and quickly convert them into quantitative outputs of cell sizes and morphologies as an established method of measuring neuronal differentiation (82, 83). Parameters quantified with this application include number of cells, cell body area, straightness of processes, numbers of processes and branches, and a total outgrowth measurement incorporating the lengths of all processes and branches. These parameters were normalized first to the number of cells in each sample and then to the corresponding values of WT cells to give fold changes (Fig. 7B–D). Although the straightness of the processes of each cell line was unchanged (data not shown), both the average cell body area and the average total outgrowth of the *Lypla1*$^{-/-}$, *Lypla2*$^{-/-}$, and DKO cells were significantly increased compared with those of WT cells. Furthermore, the average number of processes per cell was significantly increased in the DKO cells to levels comparable to that of WT cells treated with retinoic acid. Additionally, the average total outgrowth of each LYPLA KO was comparable to that of the WT cells treated with retinoic acid.

Previous studies have shown that some LysoPLs can induce or suppress neuronal differentiation (16:0 LPC and 16:0 LPA, respectively) in Neuro2a cells (17). Both of these species are present in FBS, suggesting the possibility that the conditions used to induce differentiation in the cells (a decrease in FBS content in the culture medium from 10%

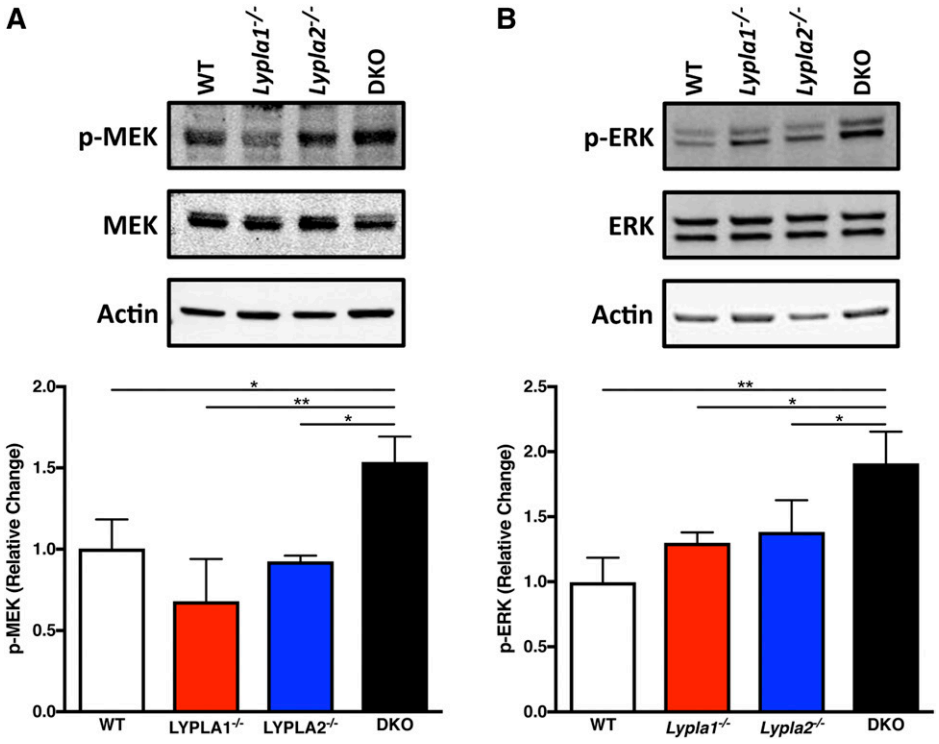

Fig. 6. Western blotting of Neuro2a lysates from WT, *Lypla1*$^{-/-}$, *Lypla2*$^{-/-}$, and DKO cells. Relative changes were quantified in triplicate analysis, and representative lanes are shown. A: Phospho-MEK1/2 (p-MEK) is significantly increased in DKO cells. B: Phospho-ERK1/2 (p-ERK) is significantly increased in DKO cells. * $P < 0.05$; ** $P < 0.01$.

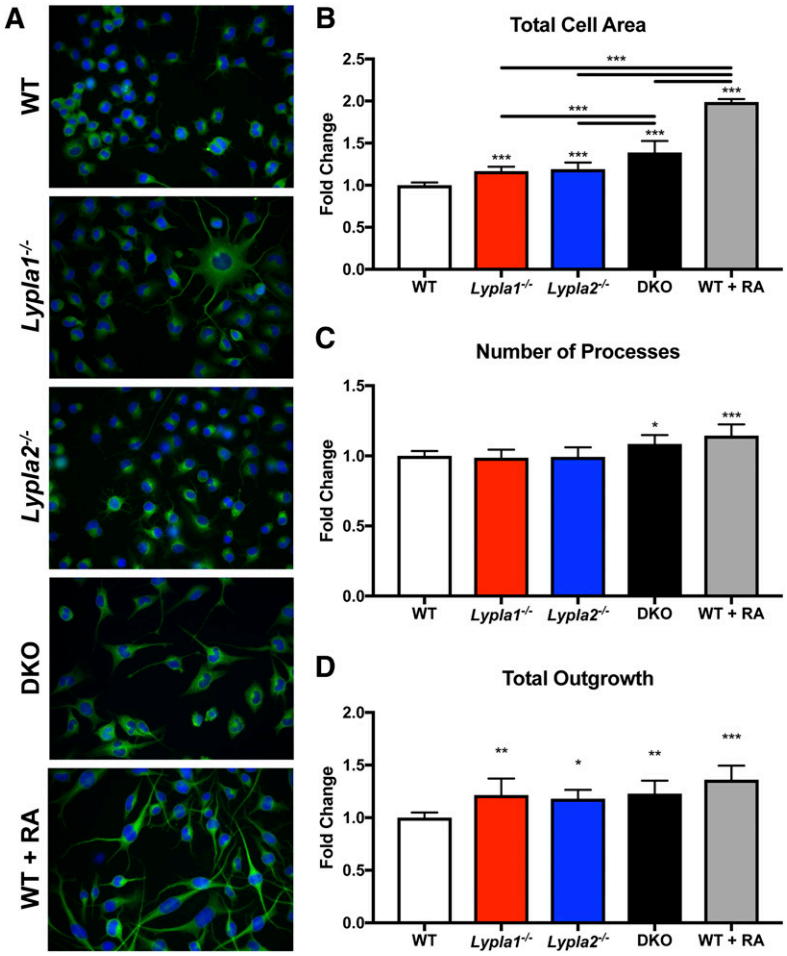

Fig. 7. KOs of *Lypla* genes induce neural differentiation. Representative images were taken from coverslips; data were quantified from images taken of 96-well plates. n = 24. A: Detection of β-III tubulin (green) and nuclei (blue) in WT, *Lypla1*$^{-/-}$, *Lypla2*$^{-/-}$, and DKO Neuro2a cells by immunocytochemistry. Cells were cultured in DMEM with 2% FBS for 48 h to induce differentiation prior to morphometric analyses using MetaXPress Imaging software. B: Average cell area normalized to WT values and represented as fold changes. C: Average number of processes per cell normalized to WT values and represented as fold changes. D: Average total outgrowth of cells normalized to WT values and represented as fold changes. * $P < 0.05$; ** $P < 0.001$; *** $P < 0.0001$.

to 2%) resulted in changes in their levels that contributed to the differentiation process. We confirmed the presence of ∼800 nM 16:0 LPC and ∼30 nM 16:0 LPA in medium containing 2% FBS, suggesting starting concentrations of ∼4 μM 16:0 LPC and ∼150 nM 16:0 LPA in medium containing 10% FBS. To directly assess the effects of these lipids on Neuro2a differentiation, we conducted experiments in which each lipid was added to differentiation medium (containing 2% FBS) at a concentration of 1 μM. The cells were not viable in the absence of serum, precluding carrying out these experiments under serum-free conditions. As shown in supplemental Fig. S5, the addition of 16:0 LPC significantly increased neuronal differentiation in each cell line, whereas the addition of 16:0 LPA had only modest effects on the average number of processes in DKO cells. These data suggest that the relatively low concentrations of LysoPLs in the 2% FBS-containing medium may be an external source of LYPLA substrates that mediate neuronal differentiation. However, the fact that concentrations of these lipids are actually decreased when the serum concentration is reduced to induce differentiation under our conditions suggests that they are unlikely to be playing a major role in the phenomena that we observe. Thus, it is most likely that higher levels of basal neuronal differentiation observed in DKO cells, which is comparable to those of WT cells treated with a differentiation agent, are due to increased endogenous LysoPL levels.

To further verify that the increased levels of neuronal differentiation were due to increased MAPK activation, WT and DKO cells were treated with a MEK inhibitor, PD98059, and neurite outgrowth parameters were quantified (**Fig. 8**). Although outgrowth parameters in cells treated with the DMSO vehicle were consistent with basal neuronal differentiation in each cell line (Fig. 7), the cell body area, number of processes, and total outgrowth of DKO cells treated with PD98059 were all significantly reduced. Furthermore, the average number of processes and total outgrowth of PD98059-treated DKO cells was comparable to that of untreated WT cells (Fig. 8C, D). These data suggest that inhibiting MAPK activation with a MEK antagonist in DKO cells counteracts the effects of increased LysoPLs on neuronal differential. The phenotypic changes to neuritogenesis, especially the increased total outgrowth of DKO cells, are likely due to the increased LysoPL levels and their role in the activation of the MAPK signaling cascade. If this is the case, LYPLAs are demonstrably important in maintaining LysoPL homeostasis and modulating their effects on signaling processes in cells.

DISCUSSION

LysoPL metabolism is a significant component of the Lands cycle, modulating the levels of potent bioactive signaling molecules and preventing membrane disruption

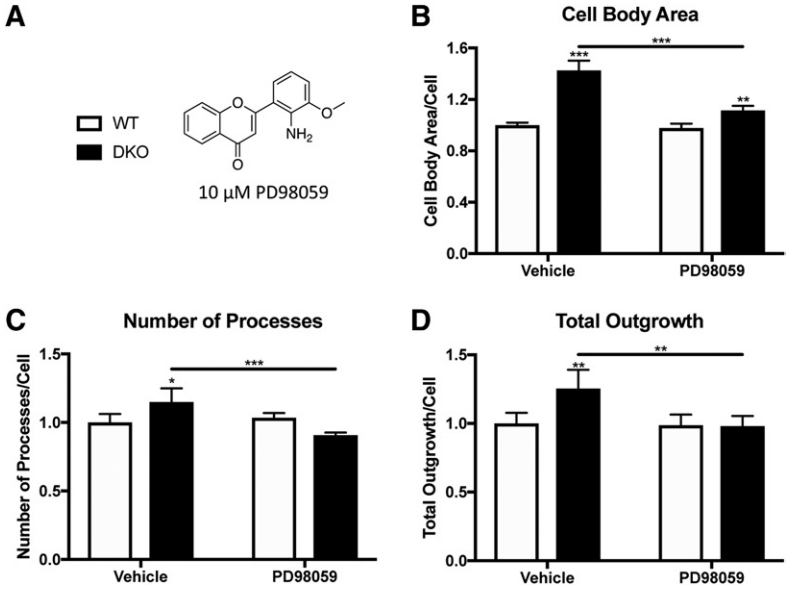

Fig. 8. PD98059 inhibition of MAPK activation reduces impact of *Lypla* KO on neuronal differentiation. Data were quantified from images taken of 96-well plates (n = 8). A: Legend of each cohort, WT cells (white) and DKO cells (black), treated with DMSO vehicle or 10 μM PD98059. B: Average cell area normalized to vehicle-treated WT values and represented as fold changes. C: Average number of processes per cell normalized to vehicle-treated WT values and represented as fold changes. D: Average total outgrowth of cells normalized to vehicle-treated WT values and represented as fold changes. * $P < 0.05$, ** $P < 0.001$; *** $P < 0.0001$.

(39, 42). LYPLA1 and LYPLA2 are responsible for a substantial fraction of this activity and, consequently, for regulating the signaling effects of their respective LysoPL substrates (32). Although past work has suggested that LYPLA1 and LYPLA2 display relative substrate specificity in terms of LysoPL hydrolysis, these studies have been done using recombinant enzyme and fail to accurately portray the roles of LYPLAs in cellular settings. To compare the activities of these two enzymes, we have taken a multifaceted approach using in vitro and cellular assays to determine how LYPLAs maintain LysoPL homeostasis.

As depicted in their crystal structures, LYPLA1 and LYPLA2 are nearly identically folded and share highly similar active sites (Fig. 2B). Accordingly, the activity of the recombinant enzymes toward the most prevalent LysoPL substrate, 16:0-LPC, is comparable (Fig. 3B). This was tested using an isotopically labeled LysoPL species, 16:0-d_3 LPC, in order to avoid contamination by the FA products of LysoPL hydrolysis. This method allows for LC/MS/MS-based quantitation of LysoPL hydrolysis without relying on expensive radiolabeled lipid substrates or purification steps that reduce sensitivity. However, to determine whether the activity of LYPLA1 and LYPLA2 toward other LysoPLs is analogous in a setting where all substrates would be available, we developed cellular models to compare their activity.

We have characterized the roles of LYPLA1 and LYPLA2 in LysoPL hydrolysis in a neuroblastoma cell model in which *Lypla1*, *Lypla2*, or both genes were deleted. The results demonstrated minimal effects of *Lypla1* deletion on LysoPL levels, although it is interesting to note that the only LysoPL species that increased in *Lypla1*$^{-/-}$ cells contained 20:4, suggesting that LYPLA1, specifically, may play a role in regulating arachidonate levels and eicosanoid biosynthesis. In contrast, *Lypla2* deletion affected a greater number and broader diversity of lipid species than *Lypla1* deletion, and substantial LysoPL elevation occurred only with KO of both enzymes (Fig. 5). In general, the data suggest that the two enzymes act cooperatively, with apparent compensation of one isoform for the loss of the other, although that occurs without substantial changes in protein expression (Fig. 4A). The consistent levels of protein expression in the KO cells suggest that the enzymes are constitutively expressed to modulate LysoPL levels. However, it is possible that the enzymes could undergo activation via posttranslational modification; both LYPLA1 and LYPLA2 are palmitoylated in cells at conserved Cys2, LYPLA1 is acetylated at Lys224, and LYPLA2 is phosphorylated at Ser82 (57, 84, 85). Nevertheless, it appears that LYPLA1 and LYPLA2 are able to hydrolyze the majority of LysoPLs in cells despite the differential preferences for LysoPL classes observed in vitro. One must interpret these data with caution, however, as lysates from DKO cells retained substantial hydrolytic activity (Fig. 4B). The specific nature of this activity is not known, but it almost certainly has an impact on the ultimate pattern of LysoPL changes observed in the various cell lines that we explored.

In neuroblastoma cells lacking both *Lypla1* and *Lypla2*, lysophospholipase activity is sufficiently compromised to lead to increased LysoPL levels (Fig. 5) and increased activation of the MAPK signaling pathway (Fig. 6). Correspondingly, these data suggest that LYPLA1 and LYPLA2 are able to modulate cell differentiation and neuritogenesis in neuroblastoma cells through their hydrolytic metabolism of LysoPLs (Fig. 7). The role of lysophospholipase-dependent modulation of LysoPL levels in physiological models of neurodifferentiation will be an interesting subject for further study.

In summary, we have closely compared the structures and activities of LYPLA1 and LYPLA2 and determined that the two proteins have significant overlap in their cellular functions. Both enzymes cooperate to maintain lipid homeostasis in cells; however, losing the activity of only one of these enzymes seems to have modest to no effect on LysoPL levels, suggesting that the counterpart lysophospholipase is able to compensate for that loss. However, when both enzymes are knocked out, the cells are unable to regulate levels of LysoPLs, leading to aberrant LysoPL-dependent signaling, an unregulated Lands cycle, and

associated phenotypic and morphological changes to the cells. This work is one of the first documented studies of LYPLA activity in a cellular setting and gives a clear answer to why inhibiting only LYPLA1 or LYPLA2 seems to have little to no effect (52, 86). We have focused here on the role of these proteins in maintaining LysoPL homeostasis, but their redundancy in substrate specificity may also apply to their other major function, namely, the thioesterase activity that results in the depalmitoylation of protein substrates (87). Although relatively few palmitoylated proteins have been identified as specific substrates for either LYPLA, it has been shown that incomplete knockdown or inhibiting only one LYPLA is ineffective, and dual inhibition of LYPLA1 and LYPLA2 with palmostatin B is often required to affect global protein palmitoylation (51, 52, 86). These trends are consistent with our findings that LYPLA1 and LYPLA2 seem to share LysoPL substrates in cells and offer credence to a dual-inhibition/KO approach to further study their physiological and pathophysiological functions.

Flow Cytometry experiments were performed in the VMC Flow Cytometry Shared Resource. The VMC Flow Cytometry Shared Resource is supported by the Vanderbilt Ingram Cancer Center (P30 CA68485) and the Vanderbilt Digestive Disease Research Center (DK058404). Antibodies were generated and purified by the Vanderbilt Antibody and Protein Resource. The Vanderbilt Antibody and Protein Resource is supported by the Vanderbilt Institute of Chemical Biology and the Vanderbilt Ingram Cancer Center (P30 CA68485). Imaging experiments were performed in the Vanderbilt High-Throughput Screening Core Facility with assistance provided by Debbie Mi and Joshua Bauer. The HTS core receives support from the Vanderbilt Institute of Chemical Biology and the Vanderbilt-Ingram Cancer Center (P30 CA68485). Statistical analyses were performed with guidance by Yu Shyr, Ph.D. from the Department of Biostatistics at Vanderbilt University.

REFERENCES

1. Makide, K., H. Kitamura, Y. Sato, M. Okutani, and J. Aoki. 2009. Emerging lysophospholipid mediators, lysophosphatidylserine, lysophosphatidylthreonine, lysophosphatidylethanolamine and lysophosphatidylglycerol. *Prostaglandins Other Lipid Mediat.* **89:** 135–139.
2. Brown, W. J., K. Chambers, and A. Doody. 2003. Phospholipase A2 (PLA2) enzymes in membrane trafficking: mediators of membrane shape and function. *Traffic.* **4:** 214–221.
3. Davidsen, J., O. G. Mouritsen, and K. Jorgensen. 2002. Synergistic permeability enhancing effect of lysophospholipids and fatty acids on lipid membranes. *Biochim. Biophys. Acta.* **1564:** 256–262.
4. Tokumura, A., M. Iimori, Y. Nishioka, M. Kitahara, M. Sakashita, and S. Tanaka. 1994. Lysophosphatidic acids induce proliferation of cultured vascular smooth muscle cells from rat aorta. *Am. J. Physiol.* **267:** C204–C210.
5. Valdés-Rives, S. A., and A. González-Arenas. 2017. Autotaxin-lysophosphatidic acid: from inflammation to cancer development. *Mediators Inflamm.* **2017:** 9173090.
6. Zhang, Y., J. D. Zhang, M. Q. Zhu, M. Zhang, Y. J. Xu, L. Cui, and N. S. Dhalla. 2017. Effect of lysophosphatidylglycerol on intracellular free Ca(2+) concentration in A10 vascular smooth muscle cells. *Can. J. Physiol. Pharmacol.* **95:** 1283–1288.
7. Drzazga, A., A. Sowinska, A. Krzeminska, P. Rytczak, M. Koziolkiewicz, and E. Gendaszewska-Darmach. 2017. Lysophosphatidylcholine elicits intracellular calcium signaling in a GPR55-dependent manner. *Biochem. Biophys. Res. Commun.* **489:** 242–247.
8. Harada, K., T. Kitaguchi, T. Kamiya, K. H. Aung, K. Nakamura, K. Ohta, and T. Tsuboi. 2017. Lysophosphatidylinositol-induced activation of the cation channel TRPV2 triggers glucagon-like peptide-1 secretion in enteroendocrine L cells. *J. Biol. Chem.* **292:** 10855–10864.
9. D'Souza, K., G. V. Paramel, and P. C. Kienesberger. 2018. Lysophosphatidic acid signaling in obesity and insulin resistance. *Nutrients.* **10:** E399.
10. Lue, H. W., J. Podolak, K. Kolahi, L. Cheng, S. Rao, D. Garg, C. H. Xue, J. K. Rantala, J. W. Tyner, K. L. Thornburg, et al. 2017. Metabolic reprogramming ensures cancer cell survival despite oncogenic signaling blockade. *Genes Dev.* **31:** 2067–2084.
11. Li, P. L., and E. Gulbins. Bioactive lipids and redox signaling: molecular mechanism and disease pathogenesis. *Antioxid. Redox Signal.* Epub ahead of print. January 24, 2018.
12. Tang, X., X. Wang, Y. Y. Zhao, J. M. Curtis, and D. N. Brindley. 2017. Doxycycline attenuates breast cancer related inflammation by decreasing plasma lysophosphatidate concentrations and inhibiting NF-kappaB activation. *Mol. Cancer.* **16:** 36.
13. Quan, H., Y. H. Hur, C. Xin, J. M. Kim, J. I. Choi, M. Y. Kim, and H. B. Bae. 2016. Stearoyl lysophosphatidylcholine enhances the phagocytic ability of macrophages through the AMP-activated protein kinase/p38 mitogen activated protein kinase pathway. *Int. Immunopharmacol.* **39:** 328–334.
14. Barnes, M. J., and J. G. Cyster. 2018. Lysophosphatidylserine suppression of T-cell activation via GPR174 requires Galphas proteins. *Immunol. Cell Biol.* **96:** 439–445.
15. Lourenssen, S., and M. G. Blennerhassett. 1998. Lysophosphatidylserine potentiates nerve growth factor-induced differentiation of PC12 cells. *Neurosci. Lett.* **248:** 77–80.
16. Cherif, H., A. Argaw, B. Cecyre, A. Bouchard, J. Gagnon, P. Javadi, S. Desgent, K. Mackie, and J. F. Bouchard. 2015. Role of GPR55 during axon growth and target innervation. *eNeuro.* **2:** ENEURO.0011-15.2015.
17. Paoletti, L., P. Domizi, H. Marcucci, A. Montaner, D. Krapf, G. Salvador, and C. Banchio. 2016. Lysophosphatidylcholine drives neuroblast cell fate. *Mol. Neurobiol.* **53:** 6316–6331.
18. Nishina, A., H. Kimura, A. Sekiguchi, R. H. Fukumoto, S. Nakajima, and S. Furukawa. 2006. Lysophosphatidylethanolamine in Grifola frondosa as a neurotrophic activator via activation of MAPK. *J. Lipid Res.* **47:** 1434–1443.
19. Callihan, P., M. W. Ali, H. Salazar, N. Quach, X. Wu, S. L. Stice, and S. B. Hooks. 2014. Convergent regulation of neuronal differentiation and Erk and Akt kinases in human neural progenitor cells by lysophosphatidic acid, sphingosine 1-phosphate, and LIF: specific roles for the LPA1 receptor. *ASN Neuro.* **6:** 1759091414558416.
20. Ikeno, Y., N. Konno, S. H. Cheon, A. Bolchi, S. Ottonello, K. Kitamoto, and M. Arioka. 2005. Secretory phospholipases A2 induce neurite outgrowth in PC12 cells through lysophosphatidylcholine generation and activation of G2A receptor. *J. Biol. Chem.* **280:** 28044–28052.
21. Khan, S. Y., N. J. McLaughlin, M. R. Kelher, P. Eckels, F. Gamboni-Robertson, A. Banerjee, and C. C. Silliman. 2010. Lysophosphatidylcholines activate G2A inducing G(alphai)(-)(1)-/G(alphaq/)(1)(1)- Ca(2)(+) flux, G(betagamma)-Hck activation and clathrin/beta-arrestin-1/GRK6 recruitment in PMNs. *Biochem. J.* **432:** 35–45.
22. Taylor, L. A., J. Arends, A. K. Hodina, C. Unger, and U. Massing. 2007. Plasma lyso-phosphatidylcholine concentration is decreased in cancer patients with weight loss and activated inflammatory status. *Lipids Health Dis.* **6:** 17.
23. Hong, C. W., T. K. Kim, H. Y. Ham, J. S. Nam, Y. H. Kim, H. Zheng, B. Pang, T. K. Min, J. S. Jung, S. N. Lee, et al. 2010. Lysophosphatidylcholine increases neutrophil bactericidal activity by enhancement of azurophil granule-phagosome fusion via glycine.GlyR alpha 2/TRPM2/p38 MAPK signaling. *J. Immunol.* **184:** 4401–4413.
24. Matsumoto, T., T. Kobayashi, and K. Kamata. 2007. Role of lysophosphatidylcholine (LPC) in atherosclerosis. *Curr. Med. Chem.* **14:** 3209–3220.
25. Jo, S. H., S. D. Kim, J. M. Kim, H. Y. Lee, S. Y. Lee, J. W. Shim, J. Yun, D. S. Im, and Y. S. Bae. 2008. Lysophosphatidylglycerol stimulates chemotactic migration in human natural killer cells. *Biochem. Biophys. Res. Commun.* **372:** 147–151.
26. Lee, S. Y., H. Y. Lee, S. D. Kim, J. W. Shim, and Y. S. Bae. 2007. Lysophosphatidylglycerol stimulates chemotactic migration and tube formation in human umbilical vein endothelial cells. *Biochem. Biophys. Res. Commun.* **363:** 490–494.

27. Anavi-Goffer, S., G. Baillie, A. J. Irving, J. Gertsch, I. R. Greig, R. G. Pertwee, and R. A. Ross. 2012. Modulation of L-alpha-lysophosphatidylinositol/GPR55 mitogen-activated protein kinase (MAPK) signaling by cannabinoids. *J. Biol. Chem.* **287:** 91–104.
28. Zhang, W., and H. T. Liu. 2002. MAPK signal pathways in the regulation of cell proliferation in mammalian cells. *Cell Res.* **12:** 9–18.
29. Meloche, S., and J. Pouyssegur. 2007. The ERK1/2 mitogen-activated protein kinase pathway as a master regulator of the G1- to S-phase transition. *Oncogene.* **26:** 3227–3239.
30. Ge, C., G. Xiao, D. Jiang, and R. T. Franceschi. 2007. Critical role of the extracellular signal-regulated kinase-MAPK pathway in osteoblast differentiation and skeletal development. *J. Cell Biol.* **176:** 709–718.
31. Kehat, I., J. Davis, M. Tiburcy, F. Accornero, M. K. Saba-El-Leil, M. Maillet, A. J. York, J. N. Lorenz, W. H. Zimmermann, S. Meloche, et al. 2011. Extracellular signal-regulated kinases 1 and 2 regulate the balance between eccentric and concentric cardiac growth. *Circ. Res.* **108:** 176–183.
32. Wang, A., and E. A. Dennis. 1999. Mammalian lysophospholipases. *Biochim. Biophys. Acta.* **1439:** 1–16.
33. Gross, R. W., and B. E. Sobel. 1983. Rabbit myocardial cytosolic lysophospholipase. Purification, characterization, and competitive inhibition by L-palmitoyl carnitine. *J. Biol. Chem.* **258:** 5221–5226.
34. Jarvis, A. A., C. Cain, and E. A. Dennis. 1984. Purification and characterization of a lysophospholipase from human amnionic membranes. *J. Biol. Chem.* **259:** 15188–15195.
35. Lepage, N., and K. D. Roberts. 1995. Purification of lysophospholipase of human spermatozoa and its implication in the acrosome reaction. *Biol. Reprod.* **52:** 616–624.
36. Ross, B. M., and S. J. Kish. 1994. Characterization of lysophospholipid metabolizing enzymes in human brain. *J. Neurochem.* **63:** 1839–1848.
37. Zhang, Y. Y., R. A. Deems, and E. A. Dennis. 1991. Lysophospholipases I and II from P388D1 macrophage-like cell line. *Methods Enzymol.* **197:** 456–468.
38. Zhang, Y. Y., and E. A. Dennis. 1988. Purification and characterization of a lysophospholipase from a macrophage-like cell line P388D1. *J. Biol. Chem.* **263:** 9965–9972.
39. Lands, W. E. 1958. Metabolism of glycerolipides; a comparison of lecithin and triglyceride synthesis. *J. Biol. Chem.* **231:** 883–888.
40. Shindou, H., D. Hishikawa, T. Harayama, K. Yuki, and T. Shimizu. 2009. Recent progress on acyl CoA: lysophospholipid acyltransferase research. *J. Lipid Res.* **50(Suppl):** S46–S51.
41. Manna, J. D., J. A. Wepy, K. Hsu, J. W. Chang, B. F. Cravatt, and L. J. Marnett. 2014. Identification of the major prostaglandin glycerol ester hydrolase in human cancer cells. *J. Biol. Chem.* **289:** 33741–33753.
42. Yamashita, A., T. Sugiura, and K. Waku. 1997. Acyltransferases and transacylases involved in fatty acid remodeling of phospholipids and metabolism of bioactive lipids in mammalian cells. *J. Biochem.* **122:** 1–16.
43. Siess, W., K. J. Zangl, M. Essler, M. Bauer, R. Brandl, C. Corrinth, R. Bittman, G. Tigyi, and M. Aepfelbacher. 1999. Lysophosphatidic acid mediates the rapid activation of platelets and endothelial cells by mildly oxidized low density lipoprotein and accumulates in human atherosclerotic lesions. *Proc. Natl. Acad. Sci. USA.* **96:** 6931–6936.
44. Zhang, C., D. L. Baker, S. Yasuda, N. Makarova, L. Balazs, L. R. Johnson, G. K. Marathe, T. M. McIntyre, Y. Xu, G. D. Prestwich, et al. 2004. Lysophosphatidic acid induces neointima formation through PPARgamma activation. *J. Exp. Med.* **199:** 763–774.
45. Wood, P. L. 2012. Lipidomics of Alzheimer's disease: current status. *Alzheimers Res. Ther.* **4:** 5.
46. Li, Y. F., R. S. Li, S. B. Samuel, R. Cueto, X. Y. Li, H. Wang, and X. F. Yang. 2016. Lysophospholipids and their G protein-coupled receptors in atherosclerosis. *Front. Biosci.* **21:** 70–88.
47. Tsukahara, T., Y. Matsuda, and H. Haniu. 2017. Lysophospholipid-related diseases and PPARgamma signaling pathway. *Int. J. Mol. Sci.* **18:** E2730.
48. Marnett, L. J. 2009. Decoding endocannabinoid signaling. *Nat. Chem. Biol. (Landmark Ed.).* **5:** 8–9.
49. Rouzer, C. A., and L. J. Marnett. 2011. Endocannabinoid oxygenation by cyclooxygenases, lipoxygenases, and cytochromes P450: cross-talk between the eicosanoid and endocannabinoid signaling pathways. *Chem. Rev.* **111:** 5899–5921.
50. Davda, D., and B. R. Martin. 2014. Acyl protein thioesterase inhibitors as probes of dynamic S-palmitoylation. *MedChemComm.* **5:** 268–276.
51. Rusch, M., T. J. Zimmermann, M. Burger, F. J. Dekker, K. Gormer, G. Triola, A. Brockmeyer, P. Janning, T. Bottcher, S. A. Sieber, et al. 2011. Identification of acyl protein thioesterases 1 and 2 as the cellular targets of the Ras-signaling modulators palmostatin B and M. *Angew. Chem. Int. Ed. Engl.* **50:** 9838–9842.
52. Vujic, I., M. Sanlorenzo, R. Esteve-Puig, M. Vujic, A. Kwong, A. Tsumura, R. Murphy, A. Moy, C. Posch, B. Monshi, et al. 2016. Acyl protein thioesterase 1 and 2 (APT-1, APT-2) inhibitors palmostatin B, ML348 and ML349 have different effects on NRAS mutant melanoma cells. *Oncotarget.* **7:** 7297–7306.
53. Aicart-Ramos, C., R. A. Valero, and I. Rodriguez-Crespo. 2011. Protein palmitoylation and subcellular trafficking. *Biochim. Biophys. Acta.* **1808:** 2981–2994.
54. Hernandez, J. L., J. D. Majmudar, and B. R. Martin. 2013. Profiling and inhibiting reversible palmitoylation. *Curr. Opin. Chem. Biol.* **17:** 20–26.
55. Martin, B. R., C. Wang, A. Adibekian, S. E. Tully, and B. F. Cravatt. 2011. Global profiling of dynamic protein palmitoylation. *Nat. Methods.* **9:** 84–89.
56. Qanbar, R., and M. Bouvier. 2003. Role of palmitoylation/depalmitoylation reactions in G-protein-coupled receptor function. *Pharmacol. Ther.* **97:** 1–33.
57. Kong, E., S. Peng, G. Chandra, C. Sarkar, Z. Zhang, M. B. Bagh, and A. B. Mukherjee. 2013. Dynamic palmitoylation links cytosol-membrane shuttling of acyl-protein thioesterase-1 and acyl-protein thioesterase-2 with that of proto-oncogene H-ras product and growth-associated protein-43. *J. Biol. Chem.* **288:** 9112–9125.
58. Garsetti, D. E., L. E. Ozgur, M. R. Steiner, R. W. Egan, and M. A. Clark. 1992. Isolation and characterization of three lysophospholipases from the murine macrophage cell line WEHI 265.1. *Biochim. Biophys. Acta.* **1165:** 229–238.
59. Sugimoto, H., H. Hayashi, and S. Yamashita. 1996. Purification, cDNA cloning, and regulation of lysophospholipase from rat liver. *J. Biol. Chem.* **271:** 7705–7711.
60. Sunaga, H., H. Sugimoto, Y. Nagamachi, and S. Yamashita. 1995. Purification and properties of lysophospholipase isoenzymes from pig gastric mucosa. *Biochem. J.* **308:** 551–557.
61. Long, J. Z., and B. F. Cravatt. 2011. The metabolic serine hydrolases and their functions in mammalian physiology and disease. *Chem. Rev.* **111:** 6022–6063.
62. Hsu, K. L., K. Tsuboi, A. Adibekian, H. Pugh, K. Masuda, and B. F. Cravatt. 2012. DAGLbeta inhibition perturbs a lipid network involved in macrophage inflammatory responses. *Nat. Chem. Biol.* **8:** 999–1007.
63. Hsu, K. L., K. Tsuboi, J. W. Chang, L. R. Whitby, A. E. Speers, H. Pugh, and B. F. Cravatt. 2013. Discovery and optimization of piperidyl-1,2,3-triazole ureas as potent, selective, and in vivo-active inhibitors of alpha/beta-hydrolase domain containing 6 (ABHD6). *J. Med. Chem.* **56:** 8270–8279.
64. Hachey, D. L., B. W. Patterson, P. J. Reeds, and L. J. Elsas. 1991. Isotopic determination of organic keto acid pentafluorobenzyl esters in biological fluids by negative chemical ionization gas chromatography/mass spectrometry. *Anal. Chem.* **63:** 919–923.
65. Ran, F. A., P. D. Hsu, J. Wright, V. Agarwala, D. A. Scott, and F. Zhang. 2013. Genome engineering using the CRISPR-Cas9 system. *Nat. Protoc.* **8:** 2281–2308.
66. Galligan, J. J., P. J. Kingsley, O. R. Wauchope, M. M. Mitchener, J. M. Camarillo, J. A. Wepy, P. S. Harris, K. S. Fritz, and L. J. Marnett. 2017. Quantitative analysis and discovery of lysine and arginine modifications. *Anal. Chem.* **89:** 1299–1306.
67. Zhao, Z., and Y. Xu. 2010. An extremely simple method for extraction of lysophospholipids and phospholipids from blood samples. *J. Lipid Res.* **51:** 652–659.
68. Okudaira, M., A. Inoue, A. Shuto, K. Nakanaga, K. Kano, K. Makide, D. Saigusa, Y. Tomioka, and J. Aoki. 2014. Separation and quantification of 2-acyl-1-lysophospholipids and 1-acyl-2-lysophospholipids in biological samples by LC-MS/MS. *J. Lipid Res.* **55:** 2178–2192.
69. Aaltonen, N., J. T. Laitinen, and M. Lehtonen. 2010. Quantification of lysophosphatidic acids in rat brain tissue by liquid chromatography-electrospray tandem mass spectrometry. *J. Chromatogr. B Analyt. Technol. Biomed. Life Sci.* **878:** 1145–1152.
70. Zeng, M., and J. N. Zhou. 2008. Roles of autophagy and mTOR signaling in neuronal differentiation of mouse neuroblastoma cells. *Cell. Signal.* **20:** 659–665.
71. Anghileri, E., S. Marconi, A. Pignatelli, P. Cifelli, M. Galie, A. Sbarbati, M. Krampera, O. Belluzzi, and B. Bonetti. 2008. Neuronal differentiation potential of human adipose-derived mesenchymal stem cells. *Stem Cells Dev.* **17:** 909–916.
72. Palmer, T. D., J. Takahashi, and F. H. Gage. 1997. The adult rat hippocampus contains primordial neural stem cells. *Mol. Cell. Neurosci.* **8:** 389–404.

73. Kim, B., P. S. Leventhal, A. R. Saltiel, and E. L. Feldman. 1997. Insulin-like growth factor-I-mediated neurite outgrowth in vitro requires mitogen-activated protein kinase activation. *J. Biol. Chem.* **272:** 21268–21273.
74. Riboni, L., A. Prinetti, R. Bassi, A. Caminiti, and G. Tettamanti. 1995. A mediator role of ceramide in the regulation of neuroblastoma Neuro2a cell differentiation. *J. Biol. Chem.* **270:** 26868–26875.
75. Devedjiev, Y., Z. Dauter, S. R. Kuznetsov, T. L. Jones, and Z. S. Derewenda. 2000. Crystal structure of the human acyl protein thioesterase I from a single X-ray data set to 1.5 A. *Structure.* **8:** 1137–1146.
76. Won, S. J., D. Davda, K. J. Labby, S. Y. Hwang, R. Pricer, J. D. Majmudar, K. A. Armacost, L. A. Rodriguez, C. L. Rodriguez, F. S. Chong, et al. 2016. Molecular mechanism for isoform-selective inhibition of acyl protein thioesterases 1 and 2 (APT1 and APT2). *ACS Chem. Biol.* **11:** 3374–3382.
77. Krissinel, E., and K. Henrick. 2004. Secondary-structure matching (SSM), a new tool for fast protein structure alignment in three dimensions. *Acta Crystallogr. D Biol. Crystallogr.* **60:** 2256–2268.
78. Yao, C. H., G. Y. Liu, K. Yang, R. W. Gross, and G. J. Patti. 2016. Inaccurate quantitation of palmitate in metabolomics and isotope tracer studies due to plastics. *Metabolomics.* **12:** 143.
79. Chen, R. F. 1967. Removal of fatty acids from serum albumin by charcoal treatment. *J. Biol. Chem.* **242:** 173–181.
80. Patterson, B. W., G. Zhao, N. Elias, D. L. Hachey, and S. Klein. 1999. Validation of a new procedure to determine plasma fatty acid concentration and isotopic enrichment. *J. Lipid Res.* **40:** 2118–2124.
81. Savinainen, J. R., E. Kansanen, T. Pantsar, D. Navia-Paldanius, T. Parkkari, M. Lehtonen, T. Laitinen, T. Nevalainen, A. Poso, A. L. Levonen, et al. 2014. Robust hydrolysis of prostaglandin glycerol esters by human monoacylglycerol lipase (MAGL). *Mol. Pharmacol.* **86:** 522–535.
82. Algarni, A. S., A. J. Hargreaves, and J. M. Dickenson. 2018. Activation of transglutaminase 2 by nerve growth factor in differentiating neuroblastoma cells: A role in cell survival and neurite outgrowth. *Eur. J. Pharmacol.* **820:** 113–129.
83. Sindi, R. A., W. Harris, G. Arnott, J. Flaskos, C. Lloyd Mills, and A. J. Hargreaves. 2016. Chlorpyrifos- and chlorpyrifos oxon-induced neurite retraction in pre-differentiated N2a cells is associated with transient hyperphosphorylation of neurofilament heavy chain and ERK 1/2. *Toxicol. Appl. Pharmacol.* **308:** 20–31.
84. Lundby, A., A. Secher, K. Lage, N. B. Nordsborg, A. Dmytriyev, C. Lundby, and J. V. Olsen. 2012. Quantitative maps of protein phosphorylation sites across 14 different rat organs and tissues. *Nat. Commun.* **3:** 876.
85. Rardin, M. J., J. C. Newman, J. M. Held, M. P. Cusack, D. J. Sorensen, B. Li, B. Schilling, S. D. Mooney, C. R. Kahn, E. Verdin, et al. 2013. Label-free quantitative proteomics of the lysine acetylome in mitochondria identifies substrates of SIRT3 in metabolic pathways. *Proc. Natl. Acad. Sci. USA.* **110:** 6601–6606.
86. Beck, M. W., R. S. Kathayat, C. M. Cham, E. B. Chang, and B. C. Dickinson. 2017. Michael addition-based probes for ratiometric fluorescence imaging of protein S-depalmitoylases in live cells and tissues. *Chem. Sci.* **8:** 7588–7592.
87. Zeidman, R., C. S. Jackson, and A. I. Magee. 2009. Protein acyl thioesterases (review). *Mol. Membr. Biol.* **26:** 32–41.